International Journal of Environmental Science and Technology (2024) 21:8675–8694
https://doi.org/10.1007/s13762-024-05587-8

ORIGINAL PAPER

Characterization of novel pectin zirconium tungstosilicate hybrid ion exchanger and its adsorptive remediation of environmental pollutants

S. Gupta[1] · E. Laiq[1] · U. Meraj[1] · Q. Qurtulen[1]

Received: 3 September 2023 / Revised: 8 February 2024 / Accepted: 6 March 2024 / Published online: 3 April 2024

Abstract

In the present article, pectin-supported zirconium tungstosilicate hybrid ion exchanger (PZTS) was synthesized and characterized the same using Fourier transform infrared spectroscopy, X-ray diffractometry, energy-dispersive X-ray spectroscopy, scanning electron microscopy and transmission electron microscopy. Ion exchange capacity (IEC), elution behavior and effects of eluent concentration on IEC, thermal and chemical effects on IEC and distribution studies have been performed. From these studies, it is found that PZTS has an IEC approximately equal to 1.22 meq/g which is found to be relatively higher than its inorganic counterpart zirconium tungstosilicate (ZTS). Apart from that, PZTS was discovered to be thermally stable as it possesses 42.63 % IEC of its initial value even at 500 °C. According to distribution studies, PZTS was found to be relatively higher selective for Pb^{2+}. Furthermore, based on distribution coefficient values, binary separations of metal ions were accomplished on the PZTS ion exchanger column. The applicability of PZTS was also examined for methylene blue (MB) dye removal from an aqueous solution. This experiment depicts that 0.6 g adsorbent removes approximately 97 % of the MB dye from 20 ppm dye solution at 9 pH within 80 min of mixing. The data are best fitted in Langmuir isotherm (with $R^2 = 0.9996$) and pseudo-second-order kinetic model. Thermodynamic studies show that the removal of MB by PZTS is spontaneous and exothermic. It was also determined that PZTS has antimicrobial properties against *Escherichia coli*.

Editorial responsibility: Y. Yang.

✉ E. Laiq
esmat.wc@amu.ac.in

[1] Department of Chemistry, Aligarh Muslim University, Aligarh 202002, India

Graphical Abstract

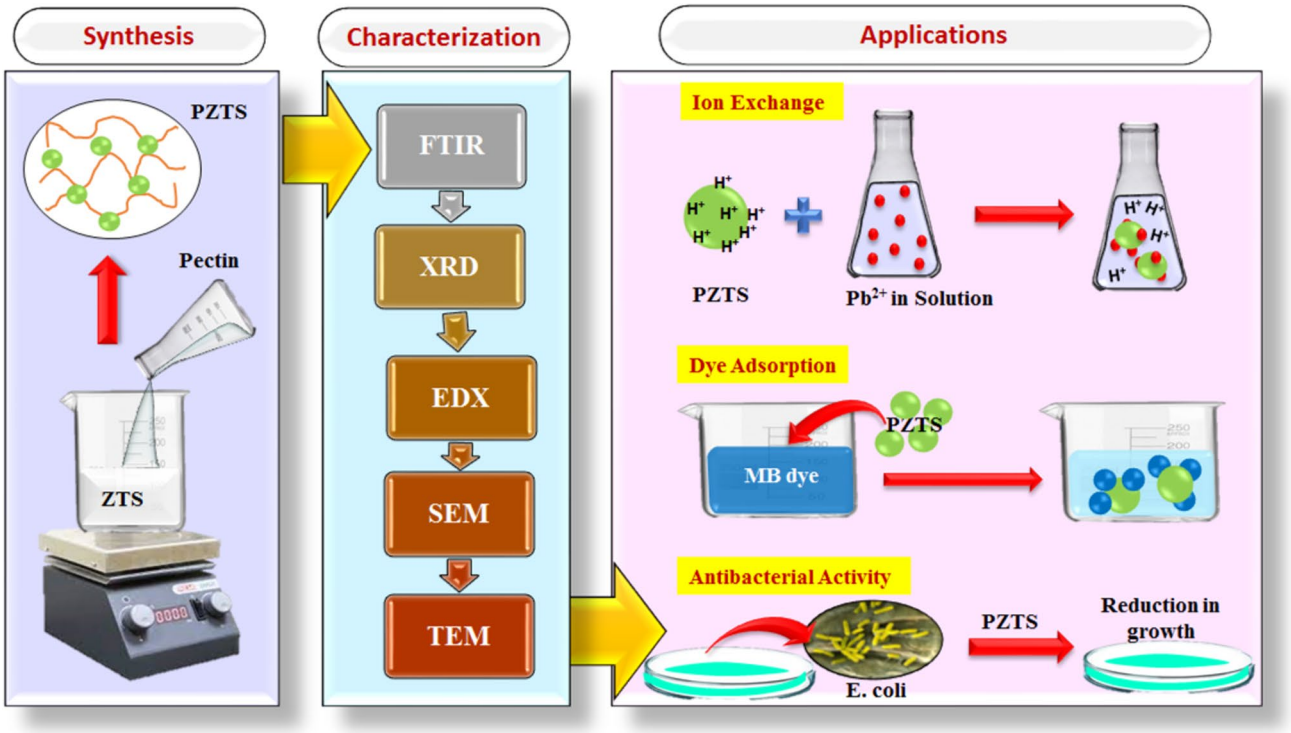

Keywords Ion exchange capacity · Distribution studies · Dye removal · Adsorption isotherms · *Escherichia coli*

Introduction

With more and more urbanization, heavy metals are discharged into the environment naturally and as well as a result of human activities. Heavy metals may derive from a variety of sources including mining, sewage discharge, industrial effluents, urban runoff, pesticides (used to treat diseases on farms), soil erosion, and more (Brevik and Bugess 2013). Although, an optimum quantity of heavy metals is required to maintain a variety of physiological and biochemical functions in living things. However, when these concentrations are exceeded beyond a certain limit, they become toxic. Despite the fact that heavy metals have been proven to have a number of adverse health effects that can last for a very long time, still, exposure to them has increased recently in numerous regions of the world. Furthermore, considering evolutionary, ecological, environmental and nutritional reasons, heavy metals can be regarded as environmental contaminants. Their toxicity is a problem that has become more and more important (Nagajyoti et al. 2010; Jaishankar et al. 2014). Other than the heavy metal ions, extensive use of various hazardous dyes (often used in the manufacturing of paper, textile, leather, and other goods) has threatened lives up to a great extent (Sarkar et al. 2011). Basically, dyes are highly carcinogenic, mutagenic, and poisonous to living organisms as their consumption has negative impacts on the respiratory system, cutaneous dermatitis, eye and mucous membrane sensitivity. Therefore, dyes and heavy metals can be the primary pollutants that are the root of extreme environmental contamination which can produce severe toxic effects. Removing these contaminants from industrial effluent is essential for reducing environmental contamination. In this regard, a variety of procedures have been investigated to remove various contaminants from waterways, including ion exchange (Hassan and Carr 2018), adsorption (Albadarin et al. 2017), electrochemical treatment (Tran et al. 2017), flotation and precipitation (Saleh et al. 2022). However, the exchange of ions and adsorption of dyes remain the most significant methods of all of these due to their effectiveness, simplicity, low cost, and ease of usage.

On one side, significant growth has been shown in the creation of ion exchangers for the removal of heavy metal

contamination from polluted poisonous water. Although, the ions can be exchanged through pure organic materials or by inorganic ion exchangers. However, they comprise some limitations in the isolated forms. The leading problem of organic resin has been its deficient thermal and chemical stability in comparison with inorganic ion exchangers, whereas the implication of inorganic ion exchangers may not be proved a useful and cost-effective solution for removing contaminants from a high volume of effluents (Siddiqui et al. 2007). To overcome all these limitations, organic–inorganic hybrid ion exchangers are synthesized due to their superior ion exchange capacity (IEC), and thermal and chemical stability. Hybrid ion exchangers exhibit a diverse set of characteristics from their constituent parts, and they are generally served as catalysts (Araad and Sasson 1989), ion exchangers (Nabi and Shalla 2009), sorbents (Vatutsina et al. 2007), and ion-selective electrodes (Khan and Alam 2003; Nabi et al. 2008). Moreover, it has also been demonstrated that biopolymer-based adsorbent materials are efficient and cost-effective for wastewater treatment. For the synthesis of such hybrid ion exchangers, zirconium-based ion exchangers have drawn a potential interest because of their outstanding ion exchange behavior in chemical science (Pathania et al.2017; Thakur et al. 2018), whereas among many organic materials, pectin grabbed substantial attention because of its sustainable and biodegradable nature. It is an organic, non-toxic amorphous carbohydrate. Moreover, the use of pectin can be tremendously appreciated for industrial and academic applications as it is widely available at a reasonable price due to its wide presence in plant tissues. So, the mixing of both of these materials (pectin and zirconium-based inorganic ion exchangers) to form a hybrid ion exchanger can be proved as one of the possible solutions for aforesaid problems.

On the other side, for the removal of unwanted dyes from water bodies, many non-traditional bio-adsorbents (including bacterial biomass or biopolymers) are being also used other than the traditional inorganic ion exchangers (Zhao et al. 2012a,b). So, adjoining the eminence of both classes of materials (organic and inorganic ion exchanger), the adsorption of dyes can become more efficient and cost-effective. In addition to the aforementioned applications, these hybrid materials are also explored for their application in antibacterial properties. Successively, this attracted the attention of numerous researchers to look at the antibacterial properties of nano-hybrid materials in opposition to microorganisms.

In this research work, the synthesis of pectin zirconium (IV) tungstosilicate (PZTS) was performed followed by the characterization, and its applications. For the structural and morphological characterization, Fourier transform infrared (FTIR) spectroscopy, X-ray diffractometry, energy-dispersive X-ray (EDX) spectroscopy, scanning electron microscopy (SEM) and transmission electron microscopy (TEM) were opted. Thereafter, distribution studies were performed to analyze the removal of various metal ions through PZTS. Experimental results of these studies specifically show the relatively higher selectivity of PZTS toward the Pb^{2+} metal ions. In accordance with the distribution studies, the binary separation of many ion groups using the column approach was done. Other than this, by making use of PZTS as an adsorbent, methylene blue (MB) dye from the water system was successfully removed. Apart from the exchanging and adsorption characteristics, this hybrid ion exchanger has shown a specific antibacterial activity toward *Escherichia coli.* This research work may be useful for the systematic studies of hybrid ion exchangers and employing the same in multi-domain applications.

Materials and methods

Reagents and materials

For these experiments, zirconium oxychloride ($ZrOCl_2.8H_2O$) and sodium tungstate ($Na_2WO_4.2H_2O$) were procured from Sigma-Aldrich. Zinc nitrate ($Zn(NO_3)_2$), nickel nitrate ($Ni(NO_3)_2$), strontium nitrate ($Sr(NO_3)_2$), ferric nitrate ($Fe(NO_3)_3$), magnesium nitrate ($Mg(NO_3)_2$), calcium nitrate ($Ca(NO_3)_2$), cobalt nitrate ($Co(NO_3)_2$), nitric acid (HNO_3), acetone (CH_3COCH_3) and MB dye ($C_{16}H_{18}ClN_3S$) were purchased from the Central Drug House. The organic polymer (pectin) was bought from Loba Chemie. Various other chemicals such as cadmium chloride ($CdCl_2$), lead nitrate ($Pb(NO_3)_2$), barium nitrate ($Ba(NO_3)_2$), ethylene diamine tetra acetic acid (EDTA), hydrochloric acid (HCl), sodium chloride (NaCl), sodium hydroxide (NaOH), potassium hydroxide (KOH), copper nitrate ($Cu(NO_3)_2$) and perchloric acid ($HClO_4$) were procured from Fisher Scientific. Acetic acid (CH_3COOH) was purchased from Merck, and sodium silicate (Na_2SiO_3) was acquired from Otto Chemie. All chemicals and reagents utilized were of the analytical grade and were employed directly.

Instrumentation

Initially, the calculated amounts of all chemicals were mixed with the help of the magnetic stirrer (2 MLH, Remi, Maharashtra, India). The suitable pH value of all desired solutions was maintained by using a digital pH meter (Meter-361, Systronics, India). For the thermal studies, a muffle furnace (Muffle Furnace, USS, India) was used which was

Table 1 Samples of the PZTS hybrid ion exchanger prepared under varied conditions

Sample no.	*A* (M)	*B* (M)	*C* (M)	*D* (wt%)	Mixing volume ratios (*A*:*B*:*C*:*D*)	The sample's appearance	IEC
S-1	0.1	0.1	0.1	–	1:1:1:0	Light yellow	0.36
S-2	0.1	0.1	0.1	–	2:1:1:0	Yellow	0.55
S-3	0.1	0.1	0.1	–	1:1:2:0	Light yellow	0. 86
S-4	0.1	0.1	0.1	–	1:2:1:0	Light yellow	0.59
S-5	0.1	0.1	0.1	1	1:1:2:1	Yellow	0.9
S-6	0.1	0.1	0.1	2	1:1:2:1	Yellowish white	1.22
S-7	0.1	0.1	0.1	3	1:1:2:1	Yellowish white	0.96
S-8	0.1	0.1	0.1	4	1:1:2:1	Yellowish white	0.95

Three replicate measurements were used to calculate the average of all numerical values in this table

Here, A represents $ZrOCl_2.8H_2O$, B represents $Na_2WO_4.2H_2O$, C represents Na_2SiO_3, and D represents pectin

operated from 100 °C to 500 °C. Various functional groups of inorganic and hybrid ion exchangers were examined through FTIR. In this technique, a KBr disk method-based FTIR spectrophotometer (Spectrum Two FTIR spectrometer, PerkinElmer, USA) working in the range 4000 cm^{-1} to 400 cm^{-1} was used to deliver the spectrum of the ion exchanger material. The studies of X-ray diffraction (XRD) were conducted by Cu-Kα radiation (wavelength is 1.54 Å) based D8 advance X-ray diffractometer (Bruker AXS Inc., U.S.A.) employing in the 2θ angle range from 5 to 80 degrees. Herein, the step time of 6.00 s was maintained along with the smoothing width and step size of 0.3° and 0.02 respectively. For the morphological studies of the ion exchangers, the SEM images were captured through a scanning electron microscope (JSM 6510LV, JEOL Ltd., Japan). The elemental composition of synthesized hybrid ion exchangers was derived from the EDX spectroscopy with 20kV accelerated voltage using the same equipment used in SEM. To analyze the particle size, a transmission electron microscope (TEM2100, JEOL Ltd., Japan) was used. To centrifugate the various mixtures, a centrifuge (REMI R-8C, REMI, India) was used. The absorbance was examined through a UV spectrophotometer (UV-2600i, Shimadzu Corporation, Japan).

Synthesis of zirconium tungstosiliate (ZTS)

ZTS was synthesized by combining 0.1 M $ZrOCl_2.8H_2O$, 0.1 M $Na_2WO_4.2H_2O$ and 0.1 M Na_2SiO_3 in different volume ratios under continuous stirring for two hours at 60 °C. Parallel to it, 0.1 M HNO_3 was added to adjust the pH of the aforementioned mixture between 0 and 1. Thereafter, the resulting precipitate was maintained overnight for digestion. Then, the precipitate was filtered through filter paper and rinsed repeatedly using double distilled water (DDW) and finally dried at 60 °C.

Synthesis of pectin zirconium tungstosilicate (PZTS) hybrid ion exchanger

To synthesize the hybrid ion exchanger, a mixture of 0.1 M $ZrOCl_2.8H_2O$, 0.1 M $Na_2WO_4.2H_2O$, and 0.1 M Na_2SiO_3 having a volume ratio of 1:1:2 was prepared on a magnetic stirrer with continual stirring. Herein, 0.1 M HNO_3 was also added to control the pH of the solution between 0 and 1. In parallel to it, 2 wt % of pectin was added to the boiling water to form a pectin-based gel. This obtained gel was mixed in the aforementioned solution under constant stirring for two hours and the resulting precipitate was maintained overnight for digestion. Afterward, the precipitate was filtered and rinsed 3–4 times with DDW and dried at 50 °C. Subsequently, the precipitate was changed into H^+ form by soaking it in 1.0 M HNO_3 for 24 h. During this process, the supernatant was replaced with fresh 1.0 M HNO_3 and performed periodic mechanical shaking. Thereafter, the extra acid was removed by filtering through filter paper and washing the precipitate with DDW in a sequential manner. Following the same process, a variety of PZTS ion exchanger samples were prepared by adjusting the amount of pectin as presented in Table 1.

Ion exchange capacity (IEC)

The IEC simply means substituting the ions available in any aqueous solution with the ions added to the exchanger. The IEC of the ion exchangers is analyzed toward the particular metal ion in a given solution to gauge the exchanger's ability to exchange a specific ion. In this experiment, the column approach was opted for IEC determination. Herein, 1.0 g of the PZTS hybrid ion exchanger in the form of H^+ ion was added on a glass wool stopper crammed at the bottom of the measuring column (consisting of an inner diameter of 0.5 cm). Thereafter, the NaCl solution was used as an eluent to exchange H^+ ions from the ion exchanger column. The exchanged H^+ ions

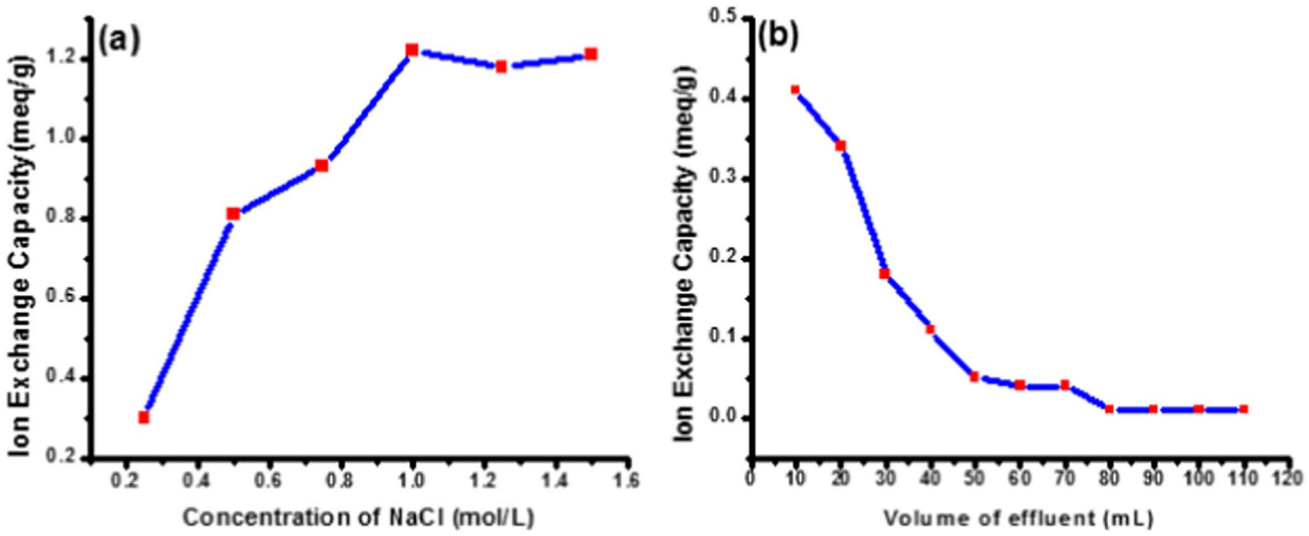

Fig. 1 **a** Effect of eluent concentration on IEC and **b** Elution behavior of PZTS ion exchanger

content was then assessed by titrating with 0.1 M NaOH. The phenolphthalein was used as an indicator. Using the weight of the exchanger and volume of NaOH, the IEC (meq/g) was calculated according to the formula given in Eq. 1.

$$\mathrm{IEC} = \frac{N \times V}{W} \mathrm{meq/g} \tag{1}$$

where N is the concentration (mol/l) and V is the volume (ml) of NaOH. Here, W is the weight of the exchanger used in grams.

IEC for different eluent concentrations and its elution behavior

The optimum concentration of the eluent needed to completely remove H^+ ions was examined by streaming various concentrations of 250 mL of NaCl solution through 1.0 g of PZTS in the form of H^+ ions placed in a glass column. The flow rate was kept constant at 1 mL per minute. Then, the effluents collected and IEC were calculated according to Eq. 1. The behavior of IEC as the function of eluent concentration is shown in Fig. 1a.

The entire elution of H^+ ions from PZTS was accomplished using a definite concentration of NaCl. By passing that definite concentration of NaCl through the column containing 1.0 g of PZTS in H^+ form, the column's efficiency was assessed. The amount of H^+ ions released in each fraction of the effluent, which was collected in 10 mL segments at a flow rate of 1.0 mL per minute, was calculated by titrating with 0.1 M NaOH Fig. 1b.

The impact of temperature on IEC

It is often observed that industrial wastewater is warm. For this reason, hybrid ion exchangers are required to be thermally stable to use in the treatment of polluted water. Therefore, the IEC of the synthesized PZTS hybrid ion exchanger was also investigated under the effect of the different temperatures. In this procedure, a muffle furnace was used for operating the ion exchanger at different temperatures ranging from 100 to 500 °C for one hour. Subsequently, after the cooling of PZTS, the IEC was assessed using the previously mentioned column approach.

Chemical stability

The chemical stability of synthesized ion exchange materials is equally essential for their applications in the desired analytical methods. Basically, the ion exchangers that are readily soluble in both acidic and water solutions might not be very helpful for separation analysis. Therefore, it is necessary to have a general idea about the solubility of an ion exchanger. In this study, 500 mg of the ion exchanger in H^+ form was treated separately with 50 mL of various solvents for 24 h and the mixtures were shaken occasionally. Thereafter, the surplus reagent was removed, and the ion exchanger was dried in an oven kept at 50 °C. Similar to the previous procedure, the IEC of the leftover material was analyzed through a column approach.

Distribution studies

The relative selectivity of the PZTS hybrid ion exchanger for different metal ions persisted in various solvents was analyzed through distribution studies. The distribution coefficient (K_d) is a useful parameter that is examined to determine the mobility of ions. Higher K_d values mean that the ion has been strongly held by the ion exchanger, while lower K_d values mean that a significant portion of the ion is still in the aqueous phase. However, the variations in K_d values depend on several other variables, including the type of metal ions, chemical bonds, concentration, pH, and solvent properties (Pisarev 2020).

Equation 2 represents the ion exchange reaction between the metal ions that interact with the PZTS ion exchanger (Taddesse et al. 2020).

$$2(\mathrm{PZTS}-\mathrm{H}) + M^{2+} \leftrightarrow (\mathrm{PZTS})_2 M + 2H^{+} \tag{2}$$

In the present article, the distribution of several metal ions was performed by using the batch approach. In this technique, 0.5 g of PZTS (in the form of H^+ ions) was mixed into 50 ml of different metallic solutions. The mixture was kept under continuous shaking for 6 to 8 h at room temperature (~ 25 ± 2 °C) to achieve the equilibrium of all mixtures. Thereafter, titration through EDTA was performed to calculate the remaining concentration of these metal ions. Initial and final concentrations of metal ions were selected for volumetric determination. The values of K_d are calculated using Eq. 3.

$$K_d = \frac{I-F}{F} \times \frac{V}{W} \tag{3}$$

where the starting volume of the EDTA titrant is "*I*" (in ml), the final volume is "*F*" (in ml), the volume of solution containing metal ions is "*V*" (in ml), and the weight of the exchanger is "*W*" (in g).

Binary separation

Primarily, the separation factor (α) was determined in order to choose the most appropriate pair for binary separation. It is described as a fraction of K_d values corresponding to two metal ions that are being separated (Gupta et al. 2023). The α can be expressed as in Eq. 4:

$$\alpha = \frac{K_d(A)}{K_d(B)} \tag{4}$$

where $K_d(A)$ and $K_d(B)$ are associated with metal ions that are being separated. The higher the value of α than unity, the higher will be the selectivity for ion A over ion B. Therefore, on the basis of α, we have selected the binary mixtures for the process of binary separation.

The column approach was again selected for the binary separation of distinct metal ions on the PZTS hybrid ion exchanger. In this method, the glass column with a glass wool support at the lower end was packed with a 1.0 g PZTS hybrid ion exchanger (in H^+ ion form). Then, the column was washed with DDW twice or thrice. Thereafter, the binary solution of distinct metal ions (that has to be separated) having 5.0 ml of each 0.02 M metal ion solution was loaded by streaming it through the glass column keeping a flow rate of 1.0 ml per minute. To ensure that all of the metal ions were completely adsorbed by PZTS, this binary solution was run through the column at least three or four times. Now, by following the distribution values of distinct metal ions in particular solvents, various eluents were applied to elute the metal ions from the hybrid ion exchanger column. Firstly, the elution of the weakly adsorbed metal ion occurs from the column as it has low K_d value in the specific solvent then elution of the strongly held metal ion (in comparison with the former) occurs as it has a higher K_d value relatively in this specific solvent. The effluents were collected in 10-ml fractions with a flow rate of 1.0 ml per minute. Thereafter, 0.01 M disodium salt of EDTA was utilized to find the metal ion concentration by the titrimetric method.

Adsorption studies

Adsorption is a phenomenon where molecules or ions attach to the surface of a solid or liquid substance. This process holds significant importance across multiple domains, encompassing chemistry, environmental science, and materials science. Different kinds of adsorption models are used to understand and predict the behavior of the adsorption process.

In the present adsorption process, the adsorption of MB dye was carried out using the batch method. Henceforth, the dye solutions with various concentrations were prepared by diluting a stock solution of 1000 ppm. Thereafter, a calibration curve was plotted by using absorbance values of standard MB dye solutions with the help of a UV–visible spectrophotometer at a wavelength of 664 nm. Various adsorption parameters such as the effect of solution pH, adsorbent doses, contact time, dye concentration and temperature were examined systematically. The adsorption of dyes was studied by adjusting these factors progressively while holding other variables constant. In this experiment, a fixed amount of adsorbent was added to 50 ml of MB dye solution in 100 ml of conical flask. When needed, the pH of the solution was maintained using HNO_3 and NaOH solution. In every experiment, the solution was agitated in a thermostatic shaker (speed 150 rpm) for a definite time

and temperature. Thereafter, the solution was centrifuged at 3000 rpm and filtered. The remaining unadsorbed MB was calculated using a UV–visible spectrophotometer. The amount of dye adsorbed on the surface of the adsorbent was calculated as percentage removal (%R) according to Eq. 5.

$$\%R = \frac{A_i - A_f}{A_i} \times 100 \tag{5}$$

where A_i represents the initial absorbance of dye before adsorption, while A_f represents absorbance after dye adsorption. Adsorption capacity (q_t) was calculated by the following formula given in Eq. 6.

$$q_t = \frac{(C_o - C_t) \times V}{m} \tag{6}$$

where C_o and C_t designate the initial concentration and remaining concentrations (after t-time) of dye in mg/l, respectively. V (l) is the volume of dye solution used, and m is the weight of adsorbent (g).

Adsorption isotherm models

Adsorption isotherms describe the relationship between the amount of adsorbate on the surface and the concentration of the adsorbate in the bulk phase. In the present article, the Langmuir and Freundlich models are mainly focused on exploring the interactions between the adsorbent and adsorbate.

(a) Langmuir adsorption isotherm model

This model is based on a few assumptions such as the adsorbent surface contains a definite number of adsorption active sites; each site on the adsorbent surface can hold only one adsorbate molecule that is adsorption is monolayer; the adsorbate molecules do not interact with each other on the adsorbent surface. In the most common way, Langmuir isotherm can be explained on the basis of surface coverage (θ) and a fraction of the vacant sites (1 − θ) (Eqs. 7 and 8).

$$K = \frac{\theta}{(1-\theta)P} \tag{7}$$

where the equilibrium constant is $\varepsilon K\varepsilon$ and the partial pressure of the gas is $\varepsilon P\varepsilon$.

$$\theta = \frac{KP}{(1+KP)} \tag{8}$$

For the solution phase, this equation takes the following form:

$$q_e = \frac{K_L C_e q_{\max}}{(1 + K_L C_e)} \tag{9}$$

This equation [Eq. 9] can also be rewritten in linear form as given through Eq. 10.

$$\frac{1}{q_e} = \frac{1}{q_{\max}} + \left(\frac{1}{q_{\max} K_L}\right)\frac{1}{C_e} \tag{10}$$

where K_L (dm^3 mol^{-1}) designates Langmuir constant and $q_{\max}$ (mg g^{-1}) designates monolayer Langmuir adsorption capacity. Equation 10 can be further rewritten in the form of Eq. 11.

$$\frac{Ce}{q_e} = \frac{Ce}{q_{\max}} + \left(\frac{1}{q_{\max} K_L}\right) \tag{11}$$

Furthermore, the separation factor R_L(that is a dimension less constant) decides whether the adsorption is unfavorable (when $R_L > 1$), linear (when $R_L = 1$), favorable (when $1 > R_L > 0$) or irreversible (when $R_L = 0$) (Kadiri et al. 2018). To calculate R_L, Eq. 12 is given.

$$R_L = \frac{1}{1 + C_i K_L} \tag{12}$$

where K_L designates Langmuir constant and C_i designates the initial dye concentration.

(b) Freundlich isotherm model

The Freundlich model can describe multilayer adsorption. This model relates the pressure of the gas to the adsorption of the adsorbate that has been given in Eq. 13.

$$q_e = K_F P^{\frac{1}{n}} \tag{13}$$

This equation [Eq. 13] can also be rewritten in the linear form as Eq. 14.

$$\log q_e = \log K_F + \frac{1}{n}\log P \tag{14}$$

For the solutions, this equation can be further modified in the form of Eq. 15.

$$\log q_e = \log K_F + \frac{1}{n}\log C_e \tag{15}$$

where q_e represents the amount of adsorbed adsorbate, and K_F represents the Freundlich constant.

Adsorption kinetics

The kinetics of adsorption processes are important for understanding the rate at which adsorption occurs. Different models may be employed to describe adsorption kinetics under specific conditions. The two primary kinetic models used in the study of adsorption are the first-order and second-order kinetics. The first-order kinetics often provides a good fit for experimental data at the initial stages of adsorption when the surface coverage is low. However, it may not accurately represent the entire adsorption process. The second-order kinetics, on the other hand, tends to be more versatile and is often a better fit for a broader range of surface coverage, including the later stages of adsorption. These models are known also as the pseudo-first-order (PFO) model and pseudo-second-order (PSO) models.

(a) Pseudo-first-order model

In accordance with this PFO model, the rate of adsorption exhibits a direct correlation with the quantity of accessible adsorption sites, as illustrated in Eq. 16..

$$\frac{\mathrm{d}q}{\mathrm{d}t} = K_f\left(q_e - q_t\right) \tag{16}$$

where q_e represents the amount of adsorbate that is adsorbed at equilibrium, q_t is the amount of adsorbate adsorbed after time t, and K_f represents the PFO rate constant. Equation 16 can be further rewritten in the linear form as Eq. 17.

$$\log\left(q_e - q_t\right) = \log q_e - \frac{K_f}{2.303}t \tag{17}$$

(b) Pseudo-second-order model

In this model, it is supposed that the chemical sorption process is a rate-determining step. Equation 18 gives a mathematical formula for this model.

$$\frac{\mathrm{d}q_t}{\mathrm{d}t} = K_s\left(q_e - q_t\right)^2 \tag{18}$$

where q_e designates the amount of adsorbed adsorbate at equilibrium, q_t is the amount of adsorbate that is adsorbed after time t, and K_s is the PSO rate constant. The linear form of this equation can be written as Eq. 19.

$$\frac{t}{q_t} = \frac{1}{k_s q_e^2} + \frac{t}{q_e} \tag{19}$$

Thermodynamic parameter

Various thermodynamic parameters of a system, including the change in Gibbs free energy (ΔG), the change in enthalpy (ΔH), and the change in entropy (ΔS), are used to examine the feasibility and type of adsorption. More specifically, by virtue of these parameters, one can gauge whether the adsorption is spontaneous or non-spontaneous, exothermic or endothermic, and increased or decreased randomness, respectively. Furthermore, these parameters can be calculated through the van't Hoff relation given in Eq. 20.

$$\ln k_c = -\frac{\Delta \mathrm{H}}{RT} + \frac{\Delta \mathrm{S}}{R} \tag{20}$$

where k_c and R are the distribution constant and the universal gas constant (= 8.314 J mol^{-1} K^{-1}), respectively and T is the temperature in Kelvin. The k_c can be further written as Eq. 21.

$$k_c = \frac{C_{\mathrm{ads}}}{C_e} \tag{21}$$

where C_{ads} (mol/L) represents the concentration of dye adsorbed on the surface of the adsorbent, and C_e (mol/L) represents the equilibrium concentration of dye.

Effect of PZTS on the growth curve of *Escherichia coli*

Escherichia coli. ATCC 25922 strain was grown in Luria–Bertani broth containing different concentrations (40 µg/mL, 60 µg/mL, 80 µg/mL and 100 µg/mL) of PZTS in 250-ml Erlenmeyer flask. Then, 1 ml of overnight grown culture of E. coli ATCC 25922 was added to each flask. The culture without any treatment was taken as a control group. The flasks were allowed to incubate at 37 °C on a shaking incubator (250 rpm). The OD at 620 nm was measured at regular intervals of 2 h to 12 h and then finally at 24 h.

Results and discussion

Synthesis and IEC analysis of hybrid ion exchanger

To synthesize the hybrid ion exchanger, it is foremost to analyze the optimum ratio of different reagents in ZTS. So, four samples (S) of distinct compositions of $ZrOCl_2.8H_2O$ (represented as A), $Na_2WO_4.2H_2O$ (represented as B) and Na_2SiO_3 (represented as C) were synthesized, and the IEC of each composition was estimated. Table 1 shows several samples with different compositions of reagents. It can be observed from this table that the volume ratio 1:1:2 (designated as

Table 2 Temperature effects on the weight, color and IEC of PZTS

Temperature (°C)	Initial wt. of sample (g)	Wt. of sample after heating (g)	Color	IEC	% Retention of IEC
100	1	0.93	Yellowish white	1.03	84.43
200	1	0.87	Light brown	0.97	79.51
300	1	0.69	Brown	0.78	63.94
400	1	0.52	Dark brown	0.69	56.56
500	1	0.43	Dark brown	0.52	42.63

At every temperature, ± 2% is the maximum deviation in % retention of IEC

Table 3 Chemical stability of PZTS in different solvents

Solvents used for chemical treatment	Weight of the exchanger before chemical treatment (mg)	Weight of the exchanger after chemical treatment (mg)	IEC (meq/g)	% Retention of IEC
0.1 M NaOH	500	387	0.93	76.23
1.0 M NaOH	500	213	0.52	42.62
0.1 M KOH	500	356	0.85	69.67
1.0 M KOH	500	208	0.51	41.80
1.0 M CH_3COOH	500	435	1.03	84.43
1.0 M CH_3COCH_3	500	451	1.09	89.34
0.1 M HNO_3	500	467	1.12	91.80
1.0 M HNO_3	500	441	1.06	86.88
2.0 M HNO_3	500	438	1.06	86.88
0.1 M HCl	500	475	1.11	90.98
1.0 M HCl	500	432	1.02	83.61
2.0 M HCl	500	419	0.99	81.15

For all solvents, ± 2% is the maximum deviation in % retention of IEC

S-3) can be considered the optimum composition of reagents in ZTS for the preparation of a hybrid ion exchanger as it serves the highest IEC (0.86 meq/g). Furthermore, as shown in Table 1, various PZTS ion exchangers have also been synthesized by varying pectin concentrations in S-3. To select the best suitable hybrid ion exchanger, their respective ion exchange potential (or IEC) has been assessed.

Table 1 clearly shows that the addition of organic moiety in ZTS certainly improves the IEC of the ion exchanger. In the present case, the IEC of the S-6 sample was figured out to be significantly greater (1.22 meq/g) in comparison with ZTS (S-3) (which is an inorganic analog of PZTS). Here, IEC is increased because the pectin (being an organic polymer) binds with an inorganic ion exchanger (ZTS) that eventually enhances the surface area of the ion exchanger and hence the number of active sites for combining the replaceable H^+ ions is increased. On the other side, further increment in pectin polymer beyond a certain concentration may cause the accumulation of active sites and that ultimately results in lower IEC. Therefore, the sample designated as S-6 was opted for the forthcoming experiments.

To figure out the appropriate concentration of eluent for completely eluting the H^+ ions from the PZTS column, eluent concentration-dependent studies were performed. Figure 1a shows the influence of eluent concentration on the overall elution of H^+ ions. It can be perceived from Fig. 1a that the entire elution of H^+ ions from the PZTS hybrid ion exchanger requires a 1.0 M concentration of the eluent (NaCl). Consequently, by using the appropriate concentration of the eluent, the pattern of elution from the exchanger was determined. Figure 1b shows the elution behavior of the PZTS hybrid ion exchanger. It is clear from the curve of Fig. 1b that most of the H^+ ions were released in approximately 90 mL of NaCl (1.0 M). It means 90 mL of eluent is sufficient for the complete elution of H^+ ions from the column which indicates the good elution behavior of the PZTS column.

To test the thermal stability of the ion exchanger, temperature-dependent IEC of the PZTS (S-6) was calculated at various temperatures ranging from 100 to 500 °C which is enlisted in Table 2. The PZTS can be considered to be thermally stable as it maintains an IEC of 42.63% up to 500 °C. However, with further increment in temperature,

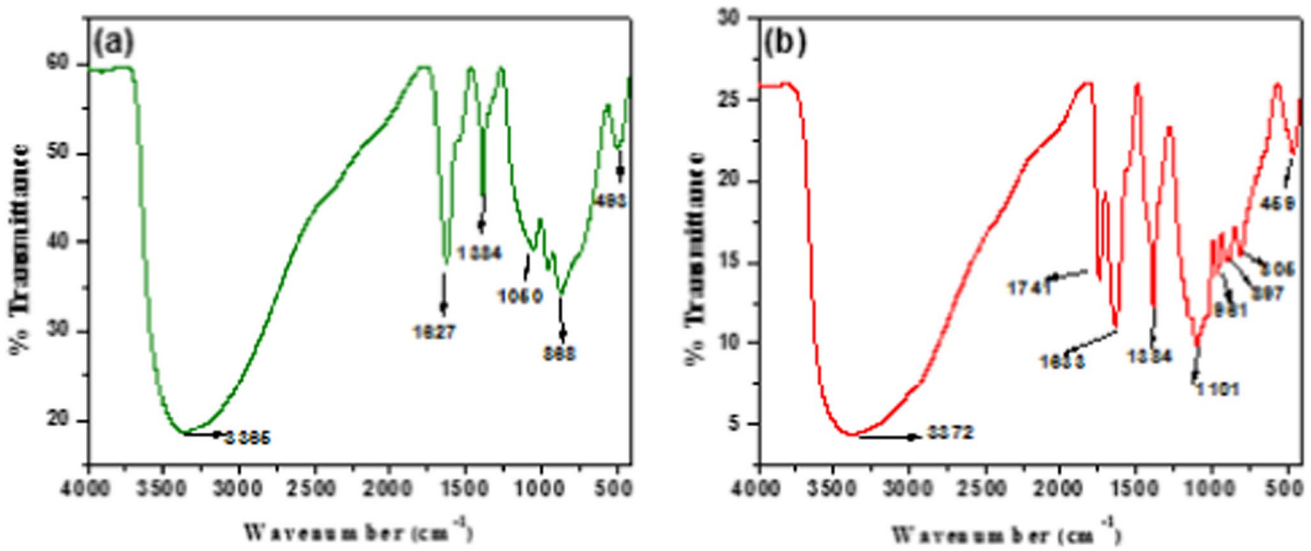

Fig. 2 FTIR spectra of **a** ZTS and **b** PZTS

a decline in IEC was observed that might be caused by the degradation of the organic counterpart of the ion exchanger. At elevated temperatures, the organic molecules that makeup part of the ion exchange material may undergo chemical reactions such as thermal degradation, oxidation, or decomposition. These reactions can lead to structural changes or breakdown of the organic matrix, compromising its ability to effectively exchange ions. As a result, the IEC diminishes over time as the temperature increases.

Table 3 illustrates the effects of different chemicals at varying concentrations on the IEC. These investigations involved the treatment of a hybrid ion exchanger with multiple acidic, basic and organic solvents for 24 h with intermittent shaking. Results showed a decrease in the weight of the ion exchanger, consequently leading to a reduction in IEC.

Table 3 shows that the synthesized ion exchanger exhibited stability when subjected to low and high concentrations of acids. The same behavior can also be observed for the organic solvents. However, it showed a tendency to dissociate in the presence of bases at all concentrations. This phenomenon could be attributed to the disruption of cross-linked networks in the presence of bases. In simpler terms, the cross-linked network acts as a holding agent of the ion exchanger together. However, when bases come into contact with the material, they weaken the connections between the polymer chains, ultimately causing the ion exchanger to break down and dissolve. This dissolution leads to a decrease in the overall IEC of the material.

Characterization of hybrid ion exchanger

Several characterization methods are utilized to evaluate structural and morphological properties. Primarily, the FTIR spectra of the ZTS and PZTS ion exchangers were examined to identify distinct functional groups that are shown in Fig. 2a and b, respectively. The wide band at 3365 cm^{-1} and the strong peak at 1627 cm^{-1} in the FTIR spectra of ZTS Fig. 2a support the existence of the –OH stretching and bending modes. The distinct band 1384 cm^{-1} is due to the presence of Si–OH which shows the presence of structural hydroxyl protons in ZTS, whereas the bands at 1050 cm^{-1} are caused by the existence of the silicate group (Rao 1963; Sadeek and Ali 2016). Additionally, the spectrum displayed bands at 868 cm^{-1}, which are indicative of the existence of the tungstate group (Sharma et al. 2014). The peak at 493 cm^{-1} represents the stretching resonance of Zr-O-Zr (Gupta et al. 2015). In the PZTS spectrum Fig. 2b, pectin's carbonyl group may be responsible for the peaks at 1741 cm^{-1} (Varshney et al. 2005). The position and intensity shift of numerous distinct peaks indicate the addition of biopolymer pectin into the inorganic component ZTS.

To characterize the crystalline/amorphous structure, phase of materials, grain size, molecular surface and orientations, general XRD is preferred. So, the XRD was performed to analyze the crystalline/amorphous nature of PZTS. Figure 3a and b displays the X-ray diffraction patterns of ZTS and PZTS. The amorphous nature of ZTS and PZTS was confirmed by the presence of low-intensity peaks. Furthermore, the hybrid ion exchanger formation was also confirmed by the change in peak intensities of PZTS compared to ZTS.

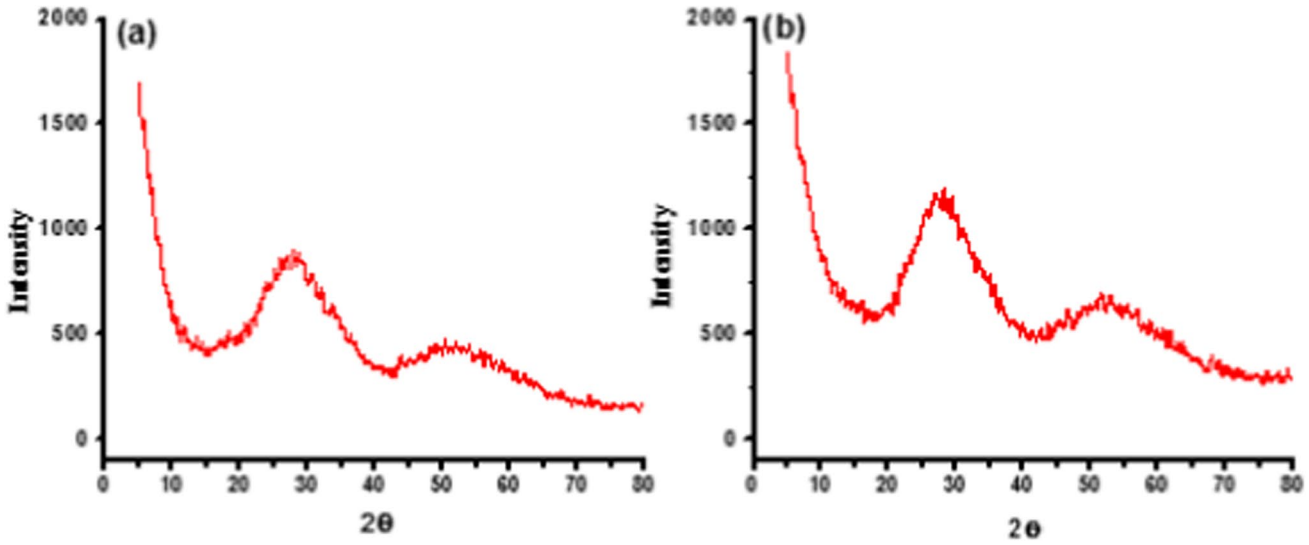

Fig. 3 XRD patterns of **a** ZTS and **b** PZTS

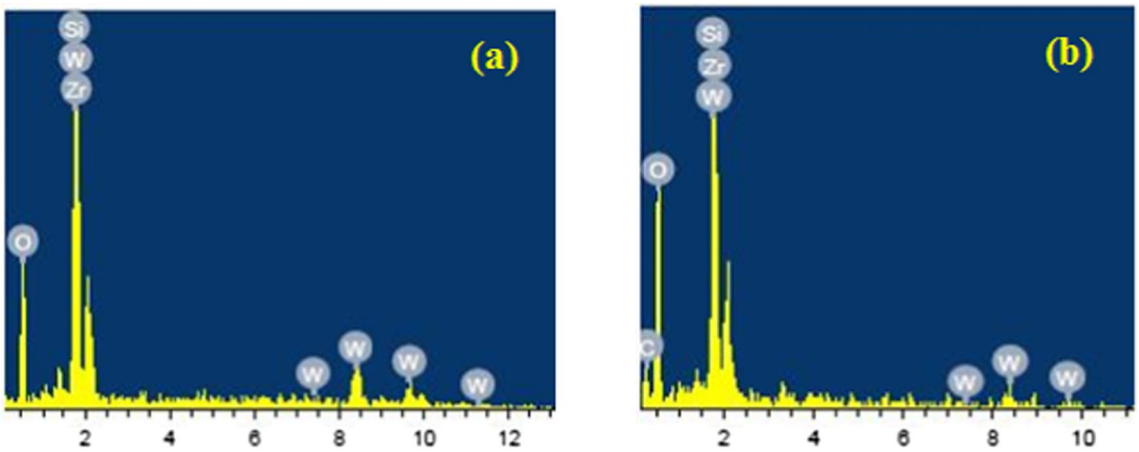

Fig. 4 EDX of **a** ZTS and **b** PZTS

EDX is performed to evaluate the elemental composition of the ZTS and PZTS ion exchangers, and the histograms of EDX are displayed in Fig. 4a and b. The synthesis of ZTS can be perceived by observing the presence of all elements, namely Zr, W, Si, and O in Fig. 4a. The inclusion of the peak corresponding to the C and O of the pectin groups in the EDX pattern of the PZTS, along with the Zr, W, Si, and O elements peaks, validates the ion exchanger' synthesis.

SEM was used to examine the morphology of the ZTS and PZTS ion exchangers. Figure 5 shows the images obtained from the SEM of ZTS (a and c) and PZTS (b and d) under various magnifications. The addition of pectin to the ZTS matrix produced noticeably distinct morphologies. ZTS's aggregated morphology can be seen on the micrograph, but PZTS has a smooth outlook with some pores. The porous character of the hybrid ion exchanger improves its surface area and adsorption capacity as well as the rate of ion exchange. Figure 5e and f, correspondingly, shows SEM scans of the PZTS hybrid ion exchanger and the MB-adsorbed PZTS hybrid ion exchanger at the same magnification. The difference between the adsorbent's SEM scans before and after the MB treatment reveals that the MB is adsorbed around the hybrid ion exchanger.

Figure 6a and b represents TEM and average particle size of the PZTS ion exchanger. The TEM of the PZTS hybrid ion exchanger confirms the average size of the particles to be in the nano-range which is approximately 36 nm. This observation establishes the PZTS material as a nanomaterial. The nano-sized particles suggest a high surface area and unique physicochemical characteristics, which can contribute to

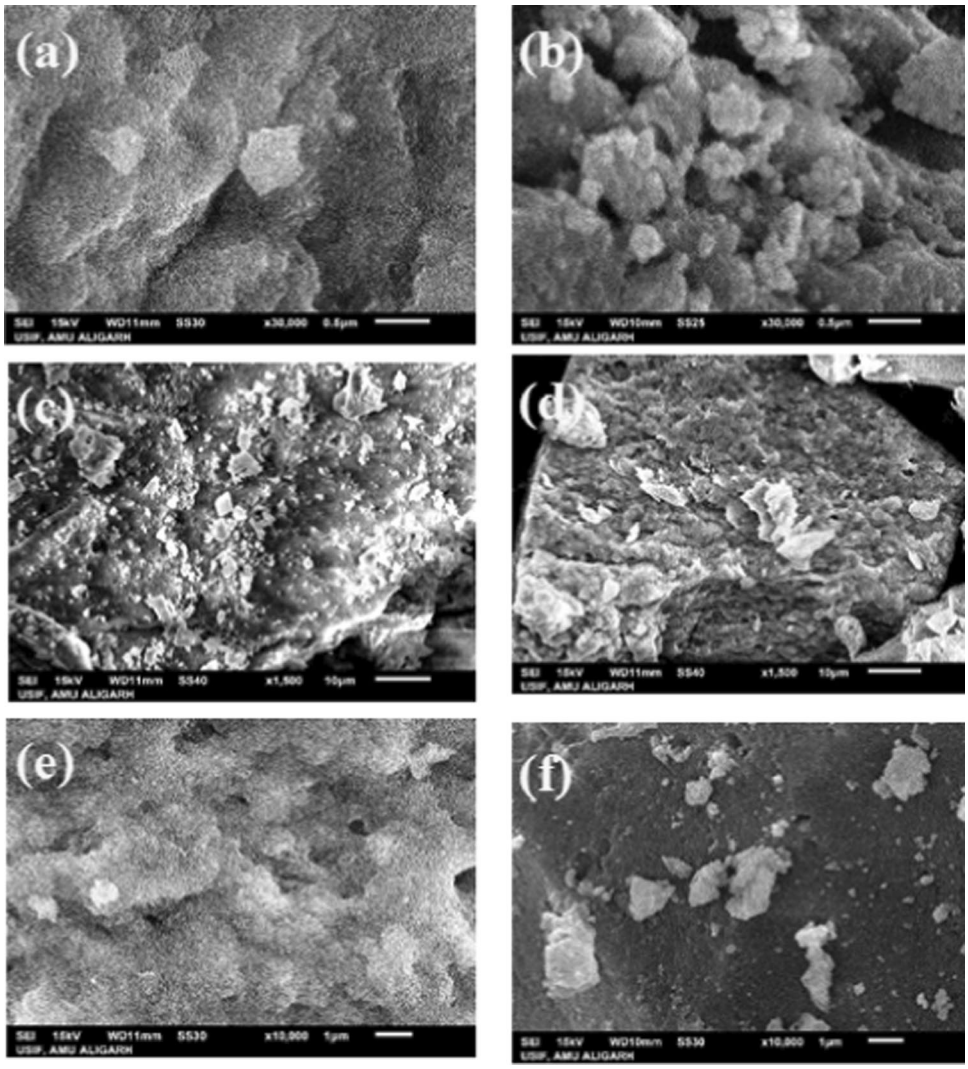

Fig. 5 SEM of ZTS (**a** and **c**), PZTS (**b** and **d**) at different magnifications and SEM of PZTS before MB adsorption (**e**) after MB adsorption (**f**)

enhanced reactivity and performance in various applications, such as adsorption or other advanced technologies.

Distribution studies and binary separation through the hybrid ion exchanger

By analyzing the distribution behavior of the PZTS, one is able to determine the selectivity of the PZTS toward the particular metal ion. So, using the batch approach (as described in Sect. "Distribution studies"), the distribution studies were carried out, and K_d values were calculated for various metal ions (Mg^{2+}, Ca^{2+}, Sr^{2+}, Ba^{2+}, Fe^{3+}, Ni^{2+}, Co^{2+}, Cu^{2+}, Zn^{2+}, Pb^{2+}, and Cd^{2+}) in various solvent systems that are shown in Table 4.

From Table 4, it can be observed that some solvents have higher K_d values (means higher sorption of metal ions), while some solvents have lower K_d values (means less sorption of metal ions). Additionally, this table shows that solvents with high concentrations as 0.1 M $HClO_4$ and 0.1 M HNO_3 have lower K_d values in comparison with solvents with low concentrations as 0.01 M $HClO_4$, 0.01 M HNO_3 and 0.001 M HNO_3. This is because of the presence of a considerable amount of H^+ ions in higher-concentration solvents which reverted the exchange process and resulted in low metal ion pickup (Thakkar and Chudasama 2009). From Table 4, comparatively high K_d values of PZTS were observed related to Pb^{2+} in each of the analyzed solvents. This can be explained by the mean of hydrated radius as the hydrated radius of a metal ion increases, the sorption of the corresponding metal ion decreases (Luca 2018). This can be the possible reason for the relatively higher selectivity of the PZTS exchanger toward the Pb^{2+}. The hydrated radius of Pb^{2+} is considered to be 4.01 Å that is the smallest hydrated radius among the studied metal ions and hence serves the highest K_d value.

The binary separation of metal ions utilizing the batch approach [discussed in Sect. "Binary separation".] based on the different K_d values of the studied metal ions (Laiq

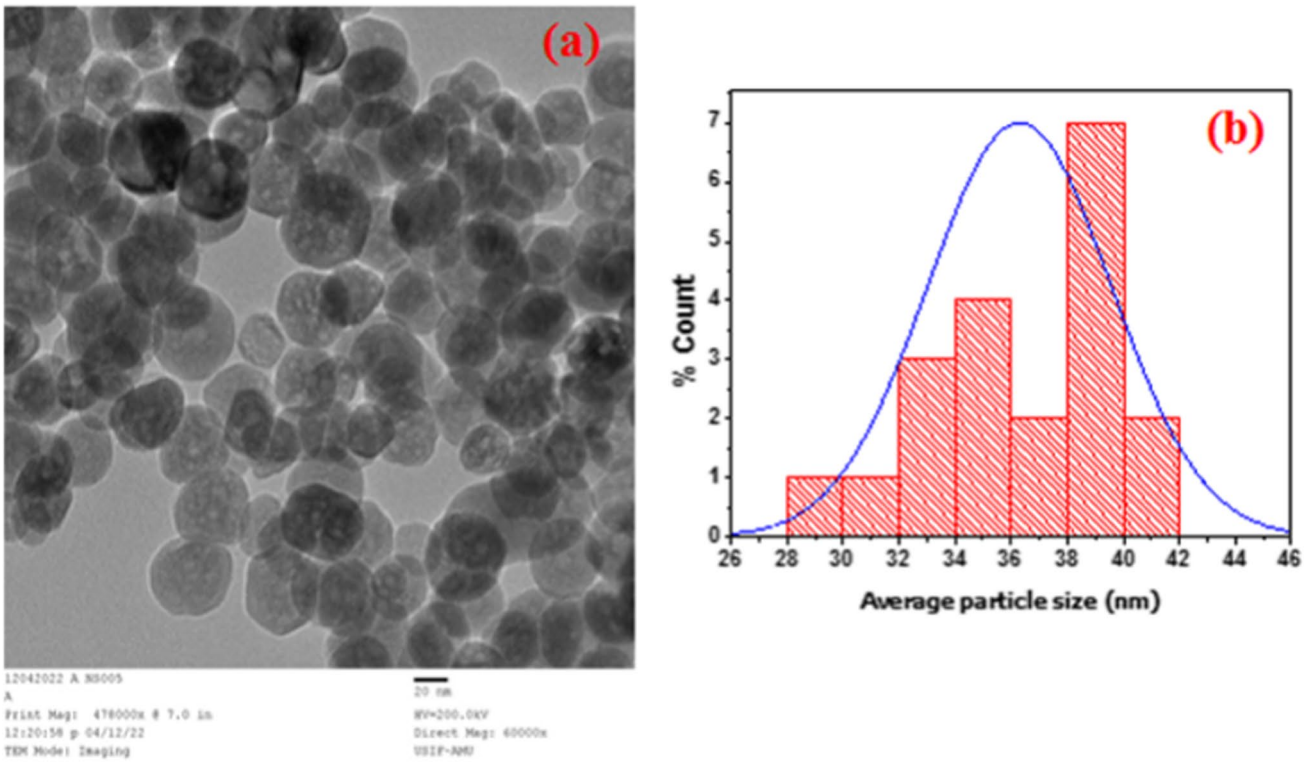

Fig. 6 **a** TEM of PZTS at 60,000 × magnification and **b** Histogram showing particle size distribution

Table 4 Distribution coefficient values for different metal ions present in different solvents on the PZTS column

Metal ions	DDW	10^{-1} M HNO_3	10^{-2} M HNO_3	10^{-3} M HNO_3	10^{-1} M $HClO_4$	10^{-2} M $HClO_4$	10^{-1} M CH_3COOH	10^{-1} M $HNO_3 + 10^{-1}$ M CH_3COOH
Mg^{2+}	498	200	257	313	197	263	371	298
Ca^{2+}	668	275	346	434	268	404	398	321
Sr^{2+}	739	328	385	522	288	419	410	358
Ba^{2+}	858	439	543	599	328	476	484	425
Fe^{3+}	100	124	217	285	79	104	52	71
Ni^{2+}	872	497	599	674	434	597	355	432
Co^{2+}	589	171	257	336	204	341	160	168
Cu^{2+}	624	252	322	400	256	397	243	264
Zn^{2+}	471	150	243	305	192	244	98	117
Pb^{2+}	1018	524	775	896	672	842	773	627
Cd^{2+}	482	158	267	324	201	253	111	126

Three replicate measurements were used to calculate the average of all numerical values in this table

Table 5 Binary separation of metal ions on PZTS column

Binary mixtures	α	Loaded amount (in mg)	Found amount (in mg)	Recovery (in %)	Eluent	Volume of eluent needed for metal ion elution (ml)
Mg^{2+}	2.04	2.43	2.02	83.02	10^{-1} M $HClO_4$	50
Pb^{2+}		20.72	18.29	88.27	10^{-1} M HNO_3	50
Fe^{3+}	10.18	5.58	5.18	92.83	10^{-1} M CH_3COOH	60
Pb^{2+}		20.72	20.16	97.30	10^{-1} M HNO_3	50
Co^{2+}	1.73	5.89	4.89	83.02	10^{-1} M CH_3COOH	50
Pb^{2+}		20.72	17.69	85.38	10^{-1} M HNO_3	50
Zn^{2+}	2.16	6.53	5.50	84.23	10^{-1} M CH_3COOH	40
Pb^{2+}		20.72	18.49	89.24	10^{-1} M HNO_3	50
Cd^{2+}	2.11	11.24	9.39	83.54	10^{-1} M CH_3COOH	60
Pb^{2+}		20.72	18.43	88.95	10^{-1} M HNO_3	50

Three replicate measurements were used to calculate the average of all numerical values in this table

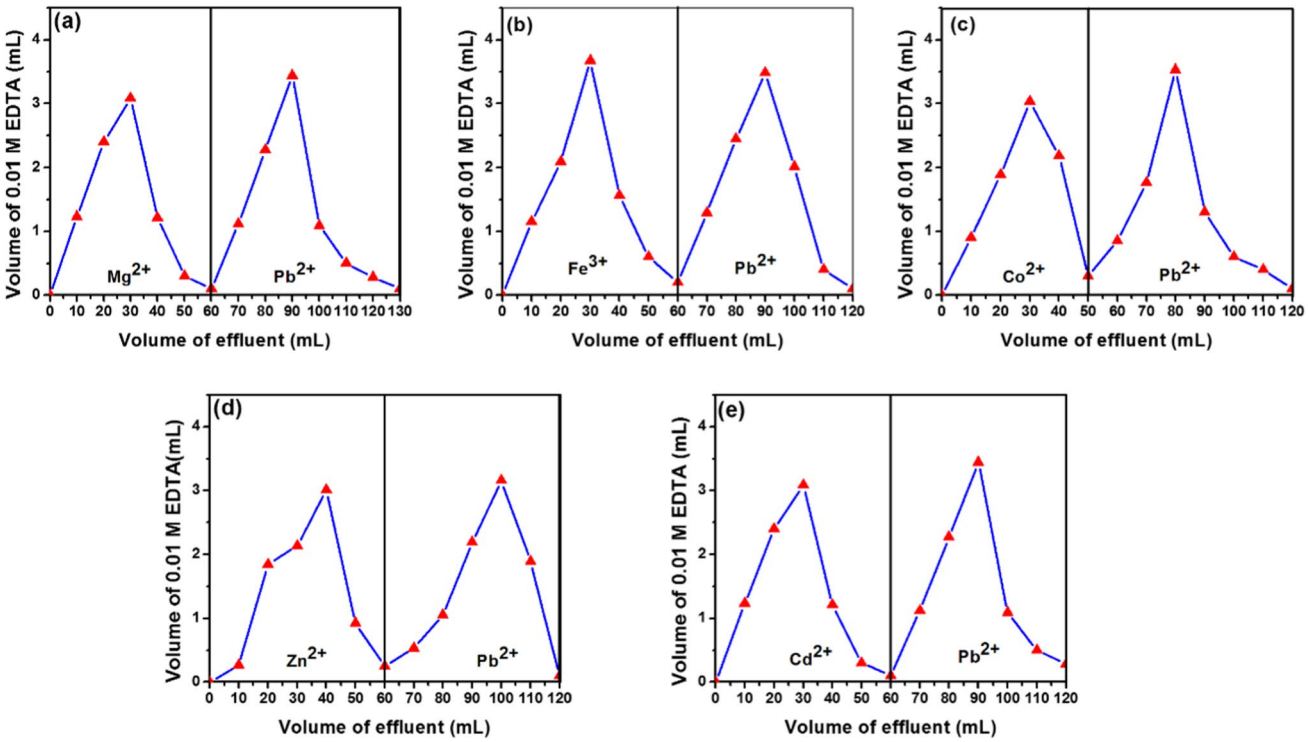

Fig. 7 Chromatograms representing the binary separation of metal ions on the PZTS ion exchanger column using different eluents

and Nabi 2021) was also performed. The α value was calculated by using the K_d values of metal ions in DDW shown in Table 4.

Now, according to the α value, five pairs of metal ions (Mg^{2+}- Pb^{2+}, Fe^{3+}- Pb^{2+}, Co^{2+}- Pb^{2+}, Zn^{2+}- Pb^{2+} and Cd^{2+}- Pb^{2+},) were utilized for binary separations, and the appropriate eluent for each metal ion and the separation sequence is given in Table 5. By applying selected eluting agents in succession, metal ions are sequentially eluted through the column to achieve separation. The metal ion that was weakly attached to the ion exchanger is eluted first and then the strongly attached metal ion by using their appropriate eluents. Therefore, a quantitative and precise recovery along with sharp separations of metal ions in all cases was found.

To calculate the amount found in each 10-mL fraction and to understand the elution behavior of eluent, the graphs between the volume of 0.01 M EDTA (in ml) and the volume of effluent (in ml) were plotted which are shown in Fig. 7. Figures 7a–e indicate that the volume of 0.01 M EDTA reaches its highest point between 20 and 30 ml of effluent volume, after which it gradually decreases.

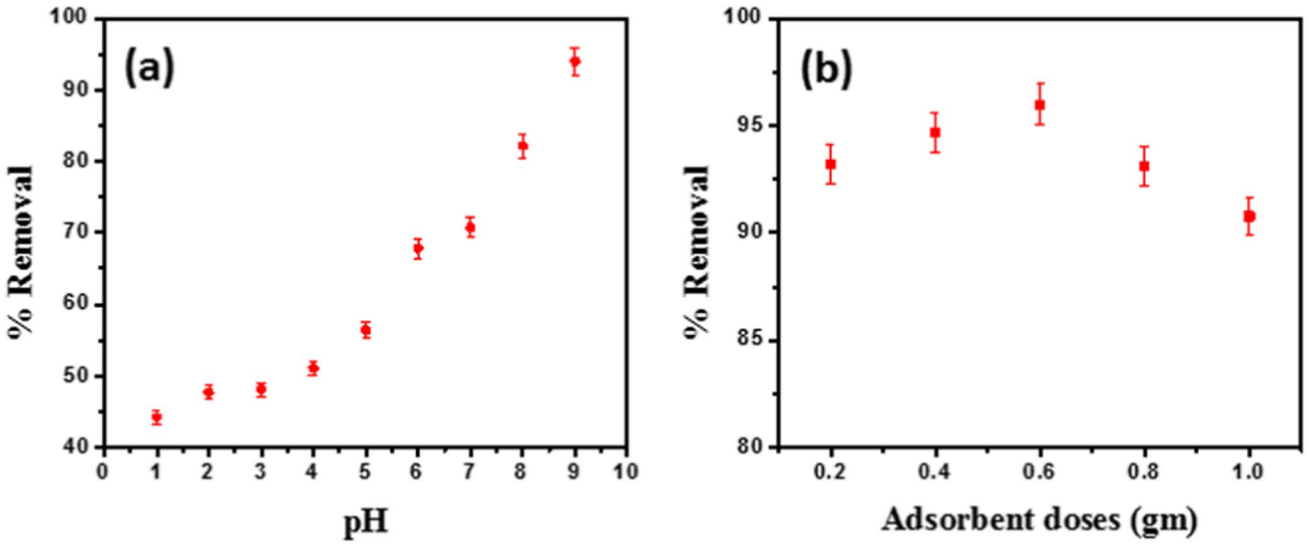

Fig. 8 Effect of **a** solution pH and **b** adsorbent doses on percentage removal

Adsorption of MB dye on PZTS hybrid ion exchanger

Effect of pH

Removal of MB dye through PZTS adsorbent was investigated at varying solution pH, adsorbent dose of 0.3 g, and dye solution of 10 ppm. For this experiment, the contact time of 60 min was also maintained at room temperature. The result found is presented in Fig. 8a. It is clear from the figure that the increment in the solution pH from 1 to 9 ultimately results in the increment of %*R*. At solution pH 9, %*R* was maximum, i.e., approximately 94 %. It may be due to the reason that on increasing pH, the nature of functional groups that are present on the surface of the adsorbent became deprotonated. Consequently, the surface of the adsorbent became more negatively charged. As it is generally known that MB is a cationic dye, it resulted in more electrostatic attraction between oppositely charged dye and adsorbent surface (Bhattacharya and Sharma 2005). Eventually, this attraction results in a higher %*R* of dye. On the other hand, at low solution pH, there is no such attraction between positively charged adsorbent and cationic MB dye. Therefore, pH 9 was considered as optimal pH for MB adsorption by PZTS adsorbent and was used for further studies.

Effect of adsorbent doses

In this experiment, the effect of different doses of adsorbent (0.2 – 1 g per 50 ml) on the MB dye within a 10 ppm dye solution at optimal pH and room temperature was studied. With the increment in adsorbent doses from 0.2 g per 50 ml to 0.6 g per 50 ml, removal of MB dye increased from approximately 93 to 96 % which is shown in Fig. 8b. This increment in %*R* with adsorbent doses may be caused by the more available adsorption sites on the surface of the adsorbent. On the other hand, no further increment was noticed in %*R* over 0.6 g per 50 ml. This may be because the conglomeration of adsorbent molecules resulted in a negligible increase in adsorbent surface area. Henceforth, 0.6 g per 50 ml can be considered as the optimal adsorbent dose for the removal of MB dye by using PZTS adsorbent and was employed for subsequent studies.

Effect of adsorbate concentration

The effect of different concentrations of adsorbate on %*R* of dye was also analyzed. To examine the removal of MB dye through the PZTS adsorbent, 0.6 g of PZTS with various concentrations (from 10 to 100 ppm) of dye was utilized at room temperature and pH 9 with a contact time of 60 min. Results given in Fig. 9a show the increment in %*R* with an increase in initial dye concentration from 10 to 20 ppm. With low concentrations of dye, there are more unoccupied adsorption sites available. On the other hand, there is a decrease in %*R* beyond 20 ppm concentration of dye as the number of available adsorption sites was decreased. Apart from this, there is also a repulsion between dye molecules that could be responsible for the decrease in %*R* of dye (Kant et al. 2014).

Effect of contact time

The contact time or exposure time of adsorbent with dye is generally defined as the time duration that is required for

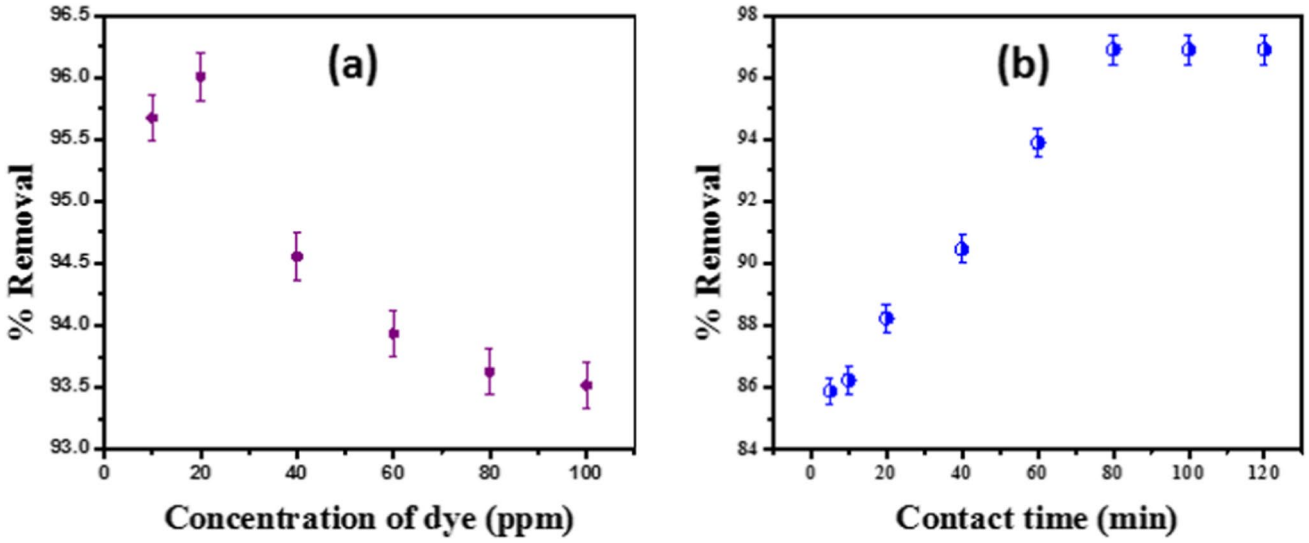

Fig. 9 Effect of **a** dye concentration and **b** contact time on percentage removal

completely adsorbing the dye on the surface of the adsorbent. An understanding of contact time can be developed by observing the *%R* of MB dye by PZTS adsorbent. To do so, various series of contact times ranging from 5 to 120 min were carefully selected with other optimum parameters at room temperature. From the results depicted in Fig. 9b, it is clear that about 96.89 % of dye was adsorbed in the time duration of 80 min, and no further significant increase in *%R* with time was observed. This can also be understood based on the vacant sites initially available on the adsorbent surface. Initially, *%R* was fast as there were more vacant adsorption sites available on the surface of the adsorbent. But after some time, all adsorption sites were filled up which sequentially led to a slight increase in *%R* (Zhang et al. 2016). Therefore, 80 min of contact time for further experiments was chosen.

Effect of temperature

The temperature can substantially affect the adsorption process as it can not only influence the surface characteristics of the adsorbent, but also the solubility and mobility of the dye molecules. So, it can also be proved a significant parameter in dye removal through PZTS. The effect of temperature on the adsorption of MB by PZTS (with other optimum parameters) is shown in Fig. 10. As the temperature increases from 20 to 60 °C percentage of MB, dye removal decreases from approximately 97 % to 82 %. Therefore, the system is considered to be exothermic. This may be due to the reason that with increasing temperature, the interaction between the MB dye molecule and active sites of adsorbent becomes weak. Moreover, the interaction between the dye and solvent becomes stronger as compared to the dye and adsorbent

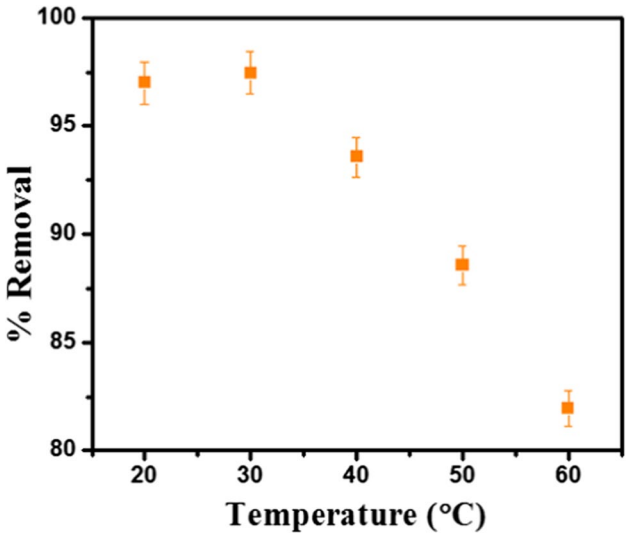

Fig. 10 Effect of temperature on percentage removal

interaction because the solubility of the dye increases in the solvent (Chandra et al. 2007).

As 97% of MB was removed by PZTS at suitable parameters, therefore, the synthesized ion exchanger PZTS is more capable of MB dye removal in comparison with the other ion exchangers such as guar gum–cerium (IV) tungstate (Gupta et al. 2014), ammonium phosphomolybdate (Joseph et al. 2019), nano-cross-linked polyacrylonitrile (Mohy Eldin et al. 2016) and grafted Holarrhena antidysenterica fiber (Kaith et al. 2015).

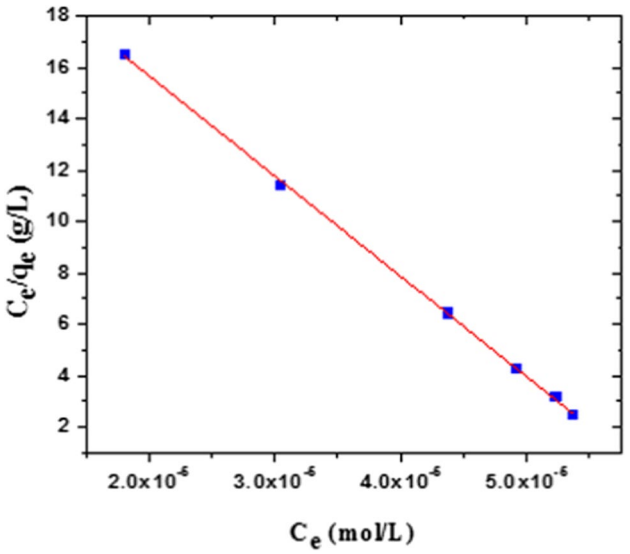

Fig. 11 Langmuir adsorption isotherm for MB removal

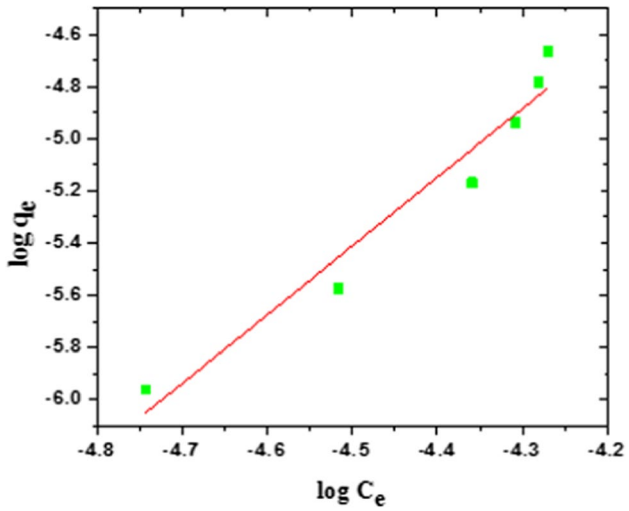

Fig. 12 Freundlich isotherm model for MB adsorption

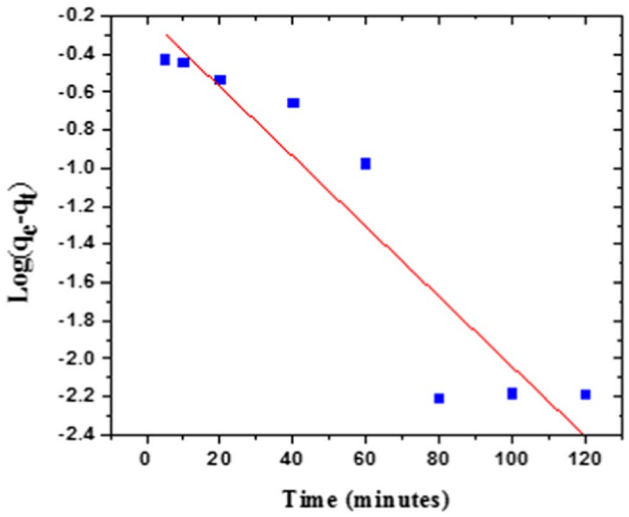

Fig. 13 Pseudo-first-order model for MB adsorption

Adsorption isotherm models

Different models are used to describe the shape of these isotherms under various conditions. The data from various concentration-based studies of adsorbate was also used to find the most suitable model for the adsorption process.

(a) Langmuir adsorption isotherm model

In the case of favorable Langmuir isotherm, a straight line is generally observed in the graph C_e/q_e versus C_e. Furthermore, the slope and intercept of this graph are used to calculate q_{max} and K_L. Data analysis of the experiments shows the appearance of a straight line in the C_e/q_e versus C_e graph as shown in Fig. 11. The value of the correlation coefficient (designated as R^2) in the case of Langmuir isotherm was found to be 0.9996. This number is very near to unity which indicates that the Langmuir adsorption process is favorable. Moreover, it is evident from the value of $R_L(=1)$ that the adsorption procedure of MB on the surface of the adsorbent is linear and favorable.

(b) Freundlich adsorption isotherm model

In the Freundlich adsorption isotherm model, a graph between $\log q_e$ versus $\log C_e$ is observed, and using the values of intercept and slope from it, K_F and n are determined. The adsorption can be considered linear when n is equal to one, a chemical process when n is smaller than one, and a physical process when n is greater than one (Shahraki et al. 2023). Figure 12 represents the Freundlich isotherm model for MB adsorption on PZTS adsorbent. From Fig. 12, it is clear that there is no linear relation between $\log q_e$ versus $\log C_e$. The value of the correlation coefficient (R^2) was found to be 0.9376 which is less than the R^2 value for the Langmuir isotherm. Therefore, it clearly indicates that the adsorption of MB follows the Langmuir isotherm and hence represents the monolayer adsorption.

Adsorption kinetics

To investigate the rate of reaction or adsorption time of MB dye on PZTS adsorbent, the adsorption kinetic models were also used.

(a) Pseudo-first-order model

Figure 13 shows a graph between $log(q_e - q_t)$ and t. The absence of a linear relationship between the variables

Table 6 Isotherm models for MB adsorption on PZTS

Langmuir adsorption isotherm model	Freundlich isotherm model
$R^2 = 0.9996$	$R^2 = 0.9376$
$R_L = 1$	$n = 0.38$
$K_L = 0.053$ (dm^3 mol^{-1})	$K_F = 625.28$ (mol g^{-1})
$q_{max} = 0.82$ (mg g^{-1})	

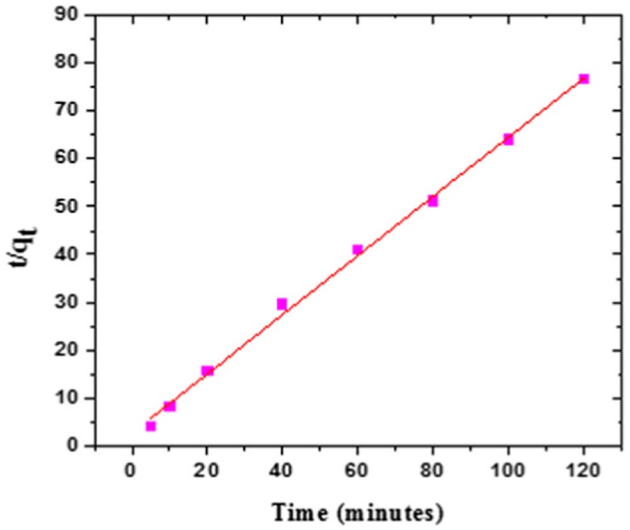

Fig. 14 Pseudo-second-order model for MB adsorption

$\log(q_e - q_t)$ and t is evident from the graph. The intercept of this graph is used to calculate q_e. Since the value of R^2 (= 0.8648) is significantly less than 1 and the calculated value of q_e is (= 0.82 mg g^{-1}) is not comparable with the experimentally observed value of q_e (= 1.56 mg g^{-1}), the PFO kinetics is not found to be appropriate for the adsorption of MB on PZTS adsorbent (Table 6).

(b) Pseudo-second-order model

Here, a straight line can be observed in the plot $\frac{t}{q_t}$ versus t in case of good agreement with the PSO model. Moreover, q_e and k_s were calculated by using the slope and intercept of this curve. A better agreement of PSO kinetics in comparison with PFO kinetics can be observed in Fig. 14 and the data analysis given in Table 7. Herein, the correlation coefficient (designated as R^2) is found to be 0.9974 which is higher than reported for a PFO model. So, this analysis shows that the PSO model is much more favorable. Moreover, the calculated q_e and experimental q_e values are very close to each other. This indicates that the adsorption of MB on the PZTS surface follows the PSO model and confirms the assumption that the dye adsorption is the result of chemisorption (Constantin et al. 2013).

Table 7 Kinetic parameters for the adsorption of MB dye on PZTS ion exchanger

PFO model	PSO model
Graph between $log(q_e - q_t)$ and t	Graph between $\frac{t}{q_t}$ and t
$R^2 = 0.8648$	$R^2 = 0.9974$
calculated $q_e = 0.82$ mg g^{-1}	calculated $q_e = 1.62$ mg g^{-1}

Table 8 Thermodynamic parameters for MB adsorption at 293 – 333 K

T (K)	ΔG (kJ mol^{-1})	ΔH (kJ mol^{-1})	ΔS (J mol^{-1} K^{-1})
293	− 0.686678611	− 51.676482	0.1396752
303	− 0.730537334		
313	− 0.478339756		
323	− 0.305173901		
333	− 0.144550776		

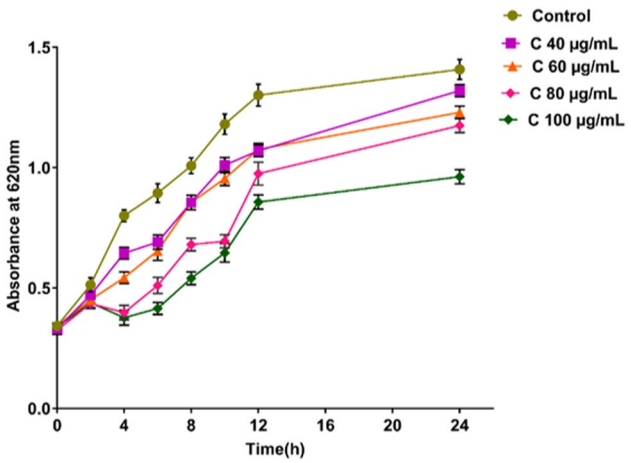

Fig. 15 Growth curve of *Escherichia coli* ATCC 25922 in presence of PZTS hybrid ion exchanger

Thermodynamic parameter

It is evident from the calculated data regarding thermodynamic parameters presented in Table 8 that the adsorption process is spontaneous in nature as the ΔG has negative values. Moreover, the negative value of ΔH proves that the process releases energy (it is an exothermic process) during dye removal. As a result, the temperature increases by the energy transfer between adsorbent and adsorbate during the adsorption process. The positive value of ΔS was also observed as randomness increases due to heat transfer. In the initial phase of adsorption, the system was more ordered as adsorbate molecules were solvated. Then, the system becomes less ordered as the adsorbate molecule adsorbed on the surface of the adsorbent by releasing the solvent molecule in the system.

Antibacterial activity of hybrid ion exchanger

Owing to the presence of various active sites, various inorganic compounds or inorganic compound-based hybrid ion exchangers are substantially explored in several biological activities (Laiq and Shahid 2021; Gupta et al. 2023). The dose-dependent inhibition of PZTS was observed on *Escherichia coli* ATCC 25922 as shown in Fig. 15. The maximum decline in optical density of culture was obtained in the presence of 100 µg/mL of concentration as compared to untreated control.

The reduction in the growth rate of *Escherichia coli* ATCC 25922 was due to a proportionately prolonged lag phase induced by increasing doses of PZTS hybrid ion exchanger in the growth medium. However, the cultures were saturated at ~ 2 h of growth as indicated by equal optical density for all doses of PZTS.

Conclusion

In this research work, a hybrid ion exchanger termed PZTS was synthesized at a specific volume ratio of 1:1:2:1 of reactants. The resulting PZTS hybrid ion exchanger displayed enhanced IEC of 1.22 meq/g, surpassing its inorganic counterpart ZTS with an IEC of 0.86 meq/g. The thermal and chemical stability of the ion exchanger was confirmed through IEC analysis at various chemical temperatures and concentrations, respectively. FTIR spectra revealed distinctive peaks affirming the synthesis of PZTS, while XRD patterns indicated its amorphous nature. SEM analyses exhibited a modification in PZTS's shape upon binding the organic polymer to ZTS. TEM analysis confirms an average particle size in the nano-range (36 nm). The selectivity of PZTS for Pb^{2+} ions was evidenced by K_d values, highlighting its potential for low-cost binary separation of Pb^{2+} ions. PZTS also demonstrated efficacy in removing MB dye, with optimal conditions identified as a 0.6 g adsorbent dose, 20 ppm dye concentration, 80 min of contact time, pH 9, and a temperature of 303 K. The examination of the adsorption isotherm model revealed that the adsorption behavior of MB on PZTS fits to the Langmuir isotherm model. Furthermore, the adsorption kinetics investigated in this study indicated that the interaction between MB dye and PZTS aligns with the PSO model. Simultaneously, the adsorption process demonstrated spontaneity and exothermic characteristics, evidenced by the negative values of ΔG and ΔH (= −51.6764). Additionally, PZTS exhibited antibacterial activity against Escherichia coli, showcasing its multifunctional capabilities. These findings underscore the promising applications of PZTS hybrid ion exchangers in environmental remediation.

Declarations

Conflict of interest Authors declare that they have no conflict of interest.

References

Albadarin AB, Collins MN, Naushad M, Shirazian S, Walker G, Mangwandi C (2017) Activated lignin–chitosan extruded blends for efficient adsorption of methylene blue. J Chem Eng 307:264–272. https://doi.org/10.1016/j.cej.2016.08.089

Arrad O, Sasson Y (1989) Commercial ion exchange resins as catalysts in solid-solid-liquid reactions. J Org Chem 54:4993–4998. https://doi.org/10.1021/jo00282a008

Bhattacharya KG, Sharma A (2005) Kinetics and thermodynamics of methylene blue adsorption on neem (Azadirachta indica) leaf powder. Dyes Pigm 65:51–59. https://doi.org/10.1016/j.dyepig.2004.06.016

Brevik EC, Burgess LC (Eds.) (2013) Soils and human health. (1st ed.). Boca Raton, CRC Press. 1–403. https://doi.org/10.1201/b13683

Chandra TC, Mirna MM, Sudaryanto Y, Ismadji S (2007) Adsorption of basic dye onto activated carbon prepared from durian shell: Studies of adsorption equilibrium and kinetics. Chem Eng J 127:121–129. https://doi.org/10.1016/j.cej.2006.09.011

Constantin M, Asmarandei I, Harabagiu V, Ghimici L, Ascenzi P, Fundueanu G (2013) Removal of anionic dyes from aqueous solutions by an ion-exchanger based on pullulan microspheres. Carbohydr Polym 91:74–84. https://doi.org/10.1016/j.carbpol.2012.08.005

Gupta VK, Pathania D, Singh P, Kumar A, Rathore BS (2014) Adsorptional removal of methylene blue by guar gum–cerium (IV) tungstate hybrid cationic exchanger. Carbohydr Polym 101:684–691. https://doi.org/10.1016/j.carbpol.2013.09.092

Gupta VK, Sharma G, Pathania D, Kothiyal NC (2015) Nanocomposite pectin Zr(IV) selenotungstophosphate for adsorptional/photocatalytic remediation of methylene blue and malachite green dyes from aqueous system. J Ind Eng Chem 21:957–964. https://doi.org/10.1016/j.jiec.2014.05.001

Gupta S, Laiq E, Meraj U (2023) A novel pectin/cerium (IV) silicomolybdate-based nanocomposite ion exchanger: preparation, characterization, and applications. Iran Polym J 32:1551–1565. https://doi.org/10.1007/s13726-023-01223-3

Hassan MM, Carr CM (2018) A critical review on recent advancements of the removal of reactive dyes from dyehouse effluent by ion-exchange adsorbents. Chemosphere 209:201–219. https://doi.org/10.1016/j.chemosphere.2018.06.043

Jaishankar M, Mathew BB, Shah MS, Murthy TPK, Gowda KRS (2014) Biosorption of few heavy metal ions using agricultural wastes. J Environ Pollut Hum Heal 2:1–6. https://doi.org/10.12691/jephh-2-1-1

Joseph J, Radhakrishnan RC, Johnson JK, Joy SP, Thomas J (2019) Ion-exchange mediated removal of cationic dye-stuffs from water using ammonium phosphomolybdate. Mater Chem Phys 242:122488. https://doi.org/10.1016/j.matchemphys.2019.122488

Kadiri L, Ouass A, Essaadaoui Y, Rifi EH, Lebkiri A (2018) Coriandrum Sativum seeds as a green low cost biosorbent for methylene blue dye removal from aqueous solution: Spectroscopic, kinetic and thermodynamic studies. Mediterr J Chem 7:204–216. https://doi.org/10.13171/mjc731810911-kadiri

Kaith BS, Dhiman J, Bhatia JK (2015) Preparation and application of grafted Holarrhena antidycentrica fiber as cation exchanger for adsorption of dye from aqueous solution. J Environ Chem Eng 3:1038–1046. https://doi.org/10.1016/j.jece.2015.03.001

Kant A, Gaijon P, Nadeem U (2014) Adsorption equilibrium and kinetics of crystal violet dye from aqueous media onto waste material. Chem Sci Rev Let 3:1–13

Khan AA, Alam MM (2003) Synthesis, characterization and analytical applications of a new and novel "organic-inorganic" composite material as a cation exchanger and Cd (II) ion-selective membrane electrode: Polyaniline Sn(IV) tungstoarsenate. React Funct Polym 55:277–290. https://doi.org/10.1016/S1381-5148(03)00018-X

Laiq E, Nabi SA (2021) Preparation, characterization and analytical application of Tin (IV) Tungstoselenate - 1, 10 Phenanthroline. Orient J Chem 37:997–1001. https://doi.org/10.13005/ojc/370430

Laiq E, Shahid N (2021) Antimicrobial activities of schiff base metal complexes of first transition series. Biosci Biotech Res Asia 18:575–583. https://doi.org/10.13005/bbra/2941

Luca PD, Bernaudo I, Elliani R, Tagarelli A, Nagy JB, Macario A (2018) Industrial waste treatment by ETS-10 ion exchanger material. Materials 11:2316. https://doi.org/10.3390/ma11112316

Mohy Eldin MS, Aggour YA, El-Aassar MR, Beghet GE, Atta RR (2016) Development of nano-crosslinked polyacrylonitrile ions exchanger particles for dyes removal. Desalin Water Treat 57:4255–4266. https://doi.org/10.1080/19443994.2014.1000383

Nabi SA, Shalla AH (2009) Synthesis, characterization and analytical application of hybrid; acrylamide zirconium (IV) arsenate a cation exchanger, effect of dielectric constant on distribution coefficient of metal ions. J Hazard Mater 163:657–664. https://doi.org/10.1016/j.jhazmat.2008.07.011

Nabi SA, Shalla AH, Ganai SA (2008) Sorption of metal ions on acrylamide zirconium (IV) arsenate and its synthesis of PVC based lead (II) selective electrode. Sep Sci Technol 43:164–178. https://doi.org/10.1080/01496390701764882

Nagajyoti PC, Lee KD, Sreekanth TVM (2010) Heavy metals, occurrence and toxicity for plants: a review. Environ Chem Lett 8:199–216. https://doi.org/10.1007/s10311-010-0297-8

Pathania D, Thakur M, Sharma A, Agarwal S, Gupta VK (2017) Synthesis of lactic acid – Zr (IV) phosphate nanocomposite ion exchanger for green remediation. Ionics (kiel) 23:699–706. https://doi.org/10.1007/s11581-016-1858-z

Pisarev OA (2020) Kinetically selective preparative chromatography of biologically active substances on polymeric sorbents. Russ Chem Bull 69:885–892. https://doi.org/10.1007/s11172-020-2845-0

Rao CNR (1963) Chemical Applications of Infrared Spectroscopy. Academic Press, New York-London

Sadeek SA, Ali IM (2016) Polyaniline based cerium phosphosilicate : synthesis, characterization and diffusion mechanism of La (III) in aqueous solutions. Bull Fac Sci Zagazig Univ 1:18–35. https://doi.org/10.21608/bfszu.2016.31063

Saleh TA, Mustaqeem M, Khaled M (2022) Water treatment technologies in removing heavy metalions from wastewater: a review. Environ Nanotechnol Monit 17:100617. https://doi.org/10.1016/j.enmm.2021.100617

Sarkar S, Chatterjee PK, Cumbal LH, SenGupta AK (2011) Hybrid ion exchanger supported nanocomposites: sorption and sensing for environmental applications. Chem Eng J 166:923–931. https://doi.org/10.1016/j.cej.2010.11.075

Shahraki HS, Ahmad A, Qurtulen GS, Meraj U (2023) Carbon dots from natural-product: applications as adsorbent and sensing of fe 3+ ions. J Inorg Organomet Polym Mater. https://doi.org/10.1007/s10904023-02707-8

Sharma G, Pathania D, Naushad M (2014) Preparation, characterization and antimicrobial activity of biopolymer based nanocomposite ion exchanger pectin zirconium (IV) selenotungstophosphate: Application for removal of toxic metals. J Ind Eng Chem 206:4482–4490. https://doi.org/10.1016/j.jiec.2014.02.020

Siddiqui WA, Khan SA, Inamuddin, (2007) Synthesis, characterization and ion-exchange properties of a new and novel "organic-inorganic" hybrid cation-exchanger: Poly(methyl methacrylate) Zr(IV) phosphate. Colloids Surf a: Physicochem Eng 295:193–199. https://doi.org/10.1016/j.colsurfa.2006.08.053

Taddesse AM, Ketema TT, Teju E (2020) Cellulose acetate-Sn(IV) molybdophosphate: a biopolymer supported composite exchanger for the removal of selected heavy metal ions. Bull Chem Soc Ethiop 34:259–276. https://doi.org/10.4314/bcse.v34i2.5

Thakkar R, Chudasama U (2009) Synthesis and characterization of zirconium titanium phosphate and its application in separation of metal ions. J Hazard Mater 172:129–137. https://doi.org/10.1016/j.jhazmat.2009.06.154

Thakur M, Pathania D, Sharma G, Naushad M, Bhatnagar A, Khan MR (2018) Synthesis, characterization and environmental applications of a new bio-composite Gelatin-Zr (IV) Phosphate. J Polym Environ 26:1415–1424. https://doi.org/10.1007/s10924-017-1043-0

Tran TK, Chiu KF, Lin CY, Leu HJ (2017) Electrochemical treatment of wastewater: Selectivity of the heavy metals removal process. Int J Hydrog Energy 42:27741–27748. https://doi.org/10.1016/j.ijhydene.2017.05.156

Varshney KG, Agrawal A, Mojumdar SC (2005) Pectin based cerium (IV) and thorium (IV) phosphates as novel hybrid fibrous ion exchangers synthesis, characterization and thermal behaviour. J Therm Anal Calorim 81:183–189. https://doi.org/10.1007/s10973-005-0765-8

Vatutsina OM, Soldatov VS, Sokolova VI, Johann J, Bissen M, Weissenbacher A (2007) A new hybrid (Polymer/inorganic) fibrous sorbent for arsenic removal from drinking water. React Funct Polym 67(184):201. https://doi.org/10.1016/j.reactfunctpolym.2006.10.009

Zhang S, Wang Z, Zhang Y, Pan H, Tao L (2016) Adsorption of methylene blue on organosolv lignin from rice straw. Procedia Environ Sci 31:3–11. https://doi.org/10.1016/j.proenv.2016.02.001

Zhao XT, Zeng T, Hu ZJ, Gao HW, Zou CY (2012a) Modeling and mechanism of the adsorption of proton onto natural bamboo sawdust. Carbohydr Polym 87:1199–1205. https://doi.org/10.1016/j.carbpol.2011.08.098

Zhao XT, Zeng T, Li XY, Hu ZJ, Gao HW, Xie Z (2012b) Modeling and mechanism of the adsorption of copper ion onto natural bamboo sawdust. Carbohydr Polym 89:185–192. https://doi.org/10.1016/j.carbpol.2012.02.069